

Expanded Exit-Pupil Holographic Head-Mounted Display With High-Speed Digital Micromirror Device

Mugeon Kim, Sungjin Lim, Geunseop Choi, Youngmin Kim, Hwi Kim, and Joonku Hahn 

Recently, techniques involving head-mounted displays (HMDs) have attracted much attention from academia and industry owing to the increased demand for virtual reality and augmented reality applications. Because HMDs are positioned near to users' eyes, it is important to solve the accommodation-vergence conflict problem to prevent dizziness. Therefore, holography is considered ideal for implementing HMDs. However, within the Nyquist region, the accommodation effect is limited by the space-bandwidth-product of the signal, which is determined by the sampling number of spatial light modulators. In addition, information about the angular spectrum is duplicated over the Fourier domain, and it is necessary to filter out the redundancy. The size of the exit-pupil of the HMD is limited by the Nyquist sampling theory. We newly propose a holographic HMD with an expanded exit-pupil over the Nyquist region by using the time-multiplexing method, and the accommodation effect is enhanced. We realize time-multiplexing by synchronizing a high-speed digital micromirror device and a liquid-crystal shutter array. We also demonstrate the accommodation effect experimentally.

Keywords: 3D displays, Color holography, Digital holography, Digital image processing, Heads-up displays.

Manuscript received Sept. 5, 2017; revised Jan. 18, 2018; accepted Feb. 5, 2018.

Mugeon Kim (im2781@gmail.com), Sungjin Lim (kslimsj0326@naver.com), Geunseop Choi (rmstjq4537@naver.com), and Joonku Hahn (corresponding author, jhahn@knu.ac.kr) are with the School of Electronics Engineering, Kyungpook National University, Daegu, Rep. of Korea.

Youngmin Kim (rainmaker@keti.re.kr) is with the VR/AR Research Center, Korea Electronics Technology Institute, Seoul, Rep. of Korea.

Hwi Kim (hwikim@korea.ac.kr) is with the Department of Electronics and Information Engineering, Korea University, Sejong, Rep. of Korea.

This is an Open Access article distributed under the term of Korea Open Government License (KOGL) Type 4: Source Indication + Commercial Use Prohibition + Change Prohibition (<http://www.kogil.or.kr/info/licenseTypeEn.do>).

I. Introduction

In recent years, head-mounted display (HMD) techniques have attracted much attention owing to the growth of the virtual reality and augmented reality market. Most HMDs provide three-dimensional (3D) images near to the human eye, and users experience 3D depth cues such as binocular disparity and convergence [1], [2]. However, 3D displays with only binocular disparity and convergence are considered to provide unnatural 3D contents, and may result in 3D sickness owing to the accommodation-vergence conflict [3]–[6]. On the other hand, digital holography reconstructs the wavefront of the object perfectly, and it is free from this conflict [7], [8]. Therefore, digital holography is considered a promising candidate for HMD applications in order to express natural 3D contents.

The image quality of digital holography is affected by the physical specifications of the spatial light modulator (SLM). The number of pixels and the pitch between them are significant parameters that contribute to characteristics of the diffracted light wave. The number of pixels is directly related to the amount of data because it represents the number of samples, which is the space-bandwidth-product (SBP). The SBP is a product of the angular spectrum of the reconstructed light wave and the size normalized by the wavelength [9]. In other words, it is impossible to increase the image size without a loss of the field of view [10]. The filtering region of the Fourier domain is defined by the Nyquist sampling theory, and the size of the viewing window is restricted by the bandwidth of angular spectrum [11]–[13]. Therefore, owing to the limited number of pixels in the SLM, it is hard to achieve an adequate field of view with a reasonable size of the viewing window.

In digital holographic displays, many researchers have proposed various methods to increase the size of the

viewing window and the field of view simultaneously. One of the most popular ways is the multiplexing technique. In spatial-multiplexing, several SLMs are used, and the use of individual optical components is usually required for each SLM [14]–[16]. Therefore, spatial multiplexing has a disadvantage when applied to HMDs owing to the difficulty in achieving a reduction in the volume and weight of the system. However, in time-multiplexing, a single SLM is usually used, and there is room to reduce the volume of the system. In addition, the number of optical components is relatively small compared with that in spatial multiplexing, and it is easier to correct the errors that result from a misalignment of the optical components [17], [18].

In this paper, we propose a holographic HMD with an exit-pupil expansion technique by using time-multiplexing. The exit-pupil expansion implies that the viewing window of the holographic display is expanded more than the Nyquist frequency determined by sampling theory. It is based on the synthetic aperture using the time-multiplexing method with a high-speed digital micromirror device (DMD) and synchronized liquid-crystal (LC) shutter array, which is used as a filter in the Fourier domain. In our proposed system, each diffracted field follows the digital holography, but every sequentially generated field is averaged in time at the eye of the observer. Therefore, the effect of the expansion is understood as a super multi-view technique. We built a compact holographic HMD that is smaller than 180 mm. In this system, the feasibility of the exit-pupil expansion technique is confirmed experimentally, and it is possible to reduce the accommodation-vergence conflict.

II. System Design

In general, digital holographic HMDs require several basic functional parts. The first one is a coherent light source, and the second one is a light modulator, while the third one is an optical filter to eliminate unwanted diffraction. The last one is an eyepiece, which is required to form a virtual image. Figure 1 shows a basic optical structure of a holographic HMD from the modulation to the eyepiece. The filter is located at the Fourier domain of the SLM plane, and $4f$ optics brings the hologram pattern on the SLM plane to the image plane. Because the image plane is positioned within the front focal length of the eyepiece, the magnified virtual image is observed through the eyepiece.

An SLM with pixel pitch, δ and N_x by N_y , pixels is assumed, and the wavefunction $U_1(x_1, y_1)$, which is the modulation by the SLM, is represented as

$$U_1(x_1, y_1) = \left[t_A(x_1, y_1) \text{comb}\left(\frac{x_1}{\delta}, \frac{y_1}{\delta}\right) \text{rect}\left(\frac{x_1}{N_x \delta}, \frac{y_1}{N_y \delta}\right) \right] \otimes \text{rect}\left(\frac{x_1}{\delta}, \frac{y_1}{\delta}\right). \quad (1)$$

Here, the DMD that is used as the SLM is a binary amplitude-only modulator, and its transmittance is given by

$$t_A(x_1, y_1) = \begin{cases} 1 & \text{if pixel is on - state} \\ 0 & \text{if pixel is off - state} \end{cases}. \quad (2)$$

Then $U_1(x_1, y_1)$ is Fourier transformed by a lens L_1 into $U_2(x_2, y_2)$. The relation between $U_1(x_1, y_1)$ and $U_2(x_2, y_2)$ is determined by

$$U_2(x_2, y_2) = \iint_{-\infty}^{\infty} U_1(x_1, y_1) \exp\left[-j \frac{2\pi}{\lambda f_1} (x_1 x_2 + y_1 y_2)\right] dx_1 dy_1. \quad (3)$$

Here, λ and f_1 are the wavelength and the focal length of the lens L_1 . In order to reconstruct the designed complex optical field, $U_2(x_2, y_2)$ needs to be filtered by passing only the single sideband because the DMD is an amplitude-only modulator. In addition, the optical filter blocks unwanted higher-order diffraction terms. After filtering, the optical wave is inversely Fourier transformed by a lens L_2 with focal length f_2 , and the wavefunction $U_3(x_3, y_3)$ at the focal plane of the lens L_2 is given by

$$U_3(x_3, y_3) = U_1\left(x_3 \frac{f_1}{f_2}, y_3 \frac{f_1}{f_2}\right). \quad (4)$$

The wavefunction $U_3(x_3, y_3)$ is an optical conjugate of $U_1(x_1, y_1)$ through $4f$ optics. Then, the virtual image of $U_3(x_3, y_3)$ is observed through the eyepiece L_3 , and consequently, the wavefunction $U_1(x_1, y_1)$ is magnified by

$$M = \frac{f_2}{f_1} \times \frac{f_3}{f_3 - d}. \quad (5)$$

Here, f_3 is the focal length of the eyepiece, and d is the distance between the $x_3 y_3$ -plane and the eyepiece. The

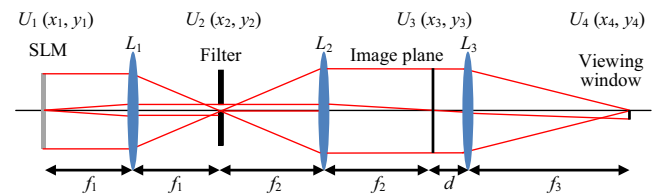


Fig. 1. Basic structure of a holographic HMD.

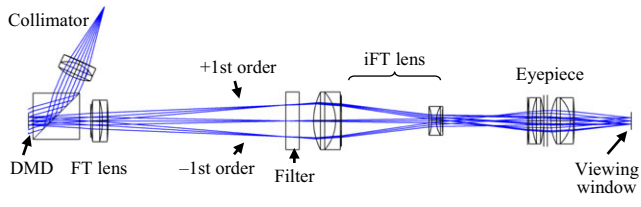


Fig. 2. Optical layout of the expanded exit-pupil holographic HMD.

viewing window (VW) is formed at the focal plane of the eyepiece, and the wavefunction at the VW is given by

$$U_4(x_4, y_4) = U_2\left(x_4 \frac{f_3}{f_2}, y_4 \frac{f_3}{f_2}\right) \exp\left[j \frac{\pi}{\lambda(Md + f_3)} (x_4^2 + y_4^2)\right]. \quad (6)$$

Here, $U_4(x_4, y_4)$ is an optical conjugate of $U_2(x_2, y_2)$. Therefore, the VW is the exit-pupil of the holographic HMD system, and it is directly related to the opening of the optical filter.

Figure 2 shows the optical layout of the expanded exit-pupil holographic HMD, which is designed based on ray optics using the program Zemax. As the light source, three light-emission diodes (LEDs) with different wavelengths, that is, red, green, and blue, are used. Partial coherence is achieved by coupling the light to a multi-mode optical fiber. The diverging light from the end of the optical fiber is collimated by a lens, and the collimated light is modulated by an SLM. Because the DMD is used as the SLM in this system, the incident wave enters the SLM obliquely at an angle of 24° . The wave modulated by the DMD passes through the prism and is Fourier transformed by the Fourier transform (FT) lens. In Fig. 2, three fields with different field angles are depicted when the DMD is in the on-state. The three fields represent the diffracted waves with different orders, and the interval between two adjacent fields corresponds to the bandwidth of the Nyquist frequency. The LC-shutter array is located on the Fourier domain, and each LC shutter is understood as a single-sideband optical filter at a specific order of diffraction. More details of optical filtering are explained in Section III. The inverse FT lens is realized by the pair of an achromatic convex lens and an achromatic concave lens. Both the convex and concave lenses are very fast, and the reason for applying a combination of them is to constrain the optical ray from getting out of the apertures of the optical components. As the eyepiece, two achromatic convex lenses are combined in order to achieve a short focal length. The focal length of the eyepiece is closely related to the field of view of the system. Through the eyepiece, the virtual image is observed at 1,000 mm away from the VW,

Table 1. Specifications of optical components.

Component	Diameter	Effective focal length
FT lens	18 mm	80 mm
Inverse FT lens 1	25 mm	40 mm
Inverse FT lens 2	12.5 mm	-25 mm
Eyepiece lens1	20 mm	60 mm
Eyepiece lens 2	20 mm	30 mm

Table 2. Specifications of head-mounted display.

System size	180 mm × 170 mm × 50 mm
Resolution	608 × 684
Image width at 1,000 mm	760 mm
Horizontal field of view	41.6°

and its width is 760 mm. Therefore, a full field of view is about 41.6° . The specifications of the optical components are summarized in Tables 1 and 2.

III. Exit-Pupil Expansion Technique and Shutter Array for Time Multiplexing

The exit-pupil expansion technique enlarges the VW such that it exceeds the limit of the Nyquist frequency. Conventionally, the VW is determined by an optical filter with a single-sideband opening. It should be noted that in rectangular array sampling, every order of diffraction is a duplication of zero-order diffraction. By using time-multiplexing, the position of the opening of the filter changes sequentially, and each opening corresponds to a single-sideband for a specific order of diffraction. As shown in Fig. 3, a DMD evaluation module manufactured by Texas Instruments is used as the SLM, and it has a DLP3000 with a native resolution of 608×684 pixels. The pixels of the DLP3000 are arranged in a rhombus shape. The diagonal length of each pixel is $10.8 \mu\text{m}$, and the pitch along its side is $7.837 \mu\text{m}$.

Each pixel of the DLP3000 is square, but the coordinates are rotated by 45° . Figure 4 shows the mapping relation for assigning a sampling point in a computer-generated hologram (CGH) to a pixel of the DMD. The data arrangement of the DMD is different from that of traditional display devices with a rectangular lattice. For example, if an image with a vertical line is loaded on the DMD, the line will become a zigzag line on the DMD. In other words, the CGH should be rearranged to enable it to be loaded on the

DMD, and a proper mapping function is necessary from the sampling space to the domain of the DMD. For sampling coordinates (x, y) , the position of the sampling point specified by (p, q) is defined by

$$p = x/\delta + 1, \tag{7}$$

$$q = -y/\delta + 1, \tag{8}$$

where δ is the sampling pitch of the pixel of the DMD, and its value is $7.837 \mu\text{m}$. Here, the region of interest at which the CGH is positioned is given by

$$343 \leq p + q \leq 1,558, \tag{9}$$

$$-342 \leq p - q \leq 342. \tag{10}$$

In the DMD coordinates (ξ, η) , the pixel of the DMD specified by (m, n) is defined by

$$m = \xi/\sqrt{2}\delta + 1 - \text{mod}(-\sqrt{2}\eta/\delta, 2)/2, \tag{11}$$

$$n = 1 - \sqrt{2}\eta/\delta. \tag{12}$$

Because the two coordinates are rotated by 45° with respect to each other, they are related by

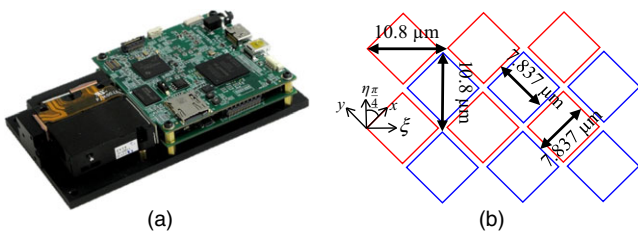


Fig. 3. (a) DMD evaluation module with DLP3000 and (b) dimensions of pixel array.

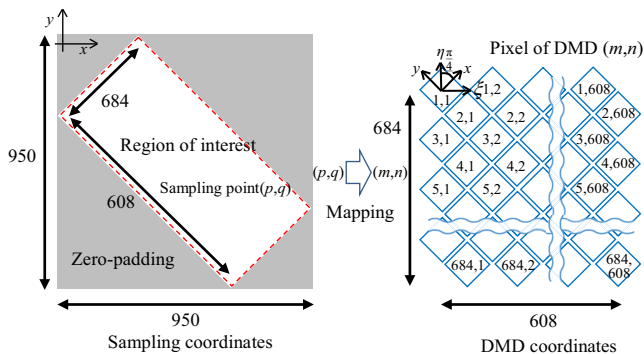


Fig. 4. Pixel mapping from sampling coordinates to DMD coordinates.

$$\begin{pmatrix} x - 341\delta \\ y \end{pmatrix} = \begin{pmatrix} 1/\sqrt{2} & -1/\sqrt{2} \\ 1/\sqrt{2} & 1/\sqrt{2} \end{pmatrix} \begin{pmatrix} \xi \\ \eta \end{pmatrix}. \tag{13}$$

As a result, the pixels of DMD (m, n) are mapped from the sampling (p, q) as follows

$$m = (p + q - 343)/2 + 1 - \text{mod}(343 - p + q, 2)/2, \tag{14}$$

$$n = 342 - p + q. \tag{15}$$

The diffraction pattern obtained by the DLP3000 is different from that of a typical SLM with an array of square-shaped pixels. In general, each pixel of the DMD has bistable positions with tilt angles of $\pm 12^\circ$. Therefore, the incident wave needs to enter obliquely by 24° , and then the reflected wave exits in a direction normal to the incident plane when the pixel is in the on-state. It should be noted that the normal direction is not an undiffracted wave, which is the D.C. term. The D.C. term appears on the other side by -24° opposite to the incident wave because the DMD can be understood as a two-dimensional (2D) blazed grating. Figure 5 shows the diffraction patterns when collimated red, green, and blue waves are diffracted by the DLP3000. The main portion of the optical power is in the normal direction owing to the tilt angle of the pixels, but the D.C. point is placed at the right side out of the captured region. In Fig. 5(a), the line with rainbow colors is the dispersion, which results from the broad spectrum of RGB LEDs. The experimental results are in good agreement with the simulation results, as shown in Fig. 5(b). Using the program Zemax, the diffraction grating is modeled and a high-order diffraction pattern is obtained after the FT lens. The higher-order diffraction terms with red (624 nm), green (515 nm), and blue (425 nm) wavelengths are depicted as points, and the

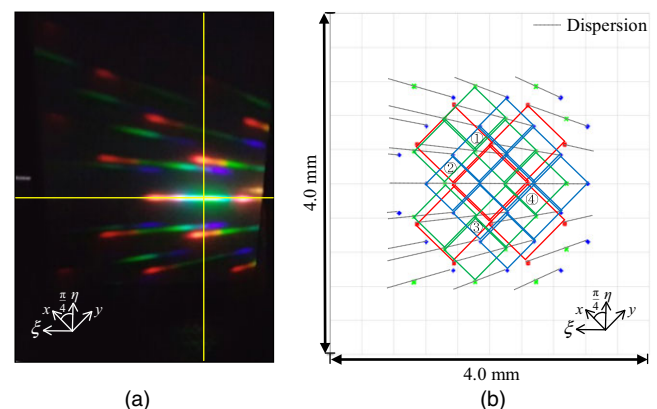


Fig. 5. Diffraction patterns of RGB waves obtained by DLP3000 in (a) experiment and (b) simulation.

color dispersions are described by dashed lines. In addition, each point is connected to identify the Nyquist region of each wavelength, and the result was in the shape of a rhombus. A suitable position for filtering is the common region of single-sidebands of high-order diffractions with RGB lights. Because the interval between diffraction orders varies according to the wavelength, it is necessary to choose the region of filtering carefully. In this study, four positions were chosen for the opening of the filter, and the circled numbers in Fig. 5(b) represent these positions.

The filter array with four apertures is made of black paper, and LC shutters are attached behind the filter array in order to control the opening individually. As the LC shutter, we used x-FOS(G2) (manufactured by LC-TEC), as shown in Fig. 6(a). Figure 6(b) shows the array of four LC shutters, where one of them is in the on-state. The LC shutter is electronically controllable, and it has a normally white mode, which means that it is transparent when no voltage is applied. The transmittance of the shutter is 2% when 5 V is applied. In this experiment, the applied voltages of the LC shutter are set to alternate between 0 V and 5 V for on and off, respectively.

Each LC shutter should be controlled in synchronization with the operation of the DMD. The LC shutters are opened sequentially according to the output trigger signal from the DMD. Figure 6(c) shows the electronic box for synchronized control of LC shutters. The electronics are functionally divided into three parts. The first part is an oscillator to provide an A.C. signal because an A.C. source (as opposed to a D.C. source) needs to be applied to the LC shutter in order to prevent the accumulation of the charge. The second part is a shifter to select one of four LC shutters sequentially according to the output trigger signal from the DMD. This part was realized with two chips such as a four-channel switch and a 4-bit binary ring-shifter. The A.C. signal from the oscillator is connected to the inputs of the switches, and these switches are controlled by the 4-bit binary ring-shifter sequentially. The 4-bit binary ring-shifter receives a pulse-type signal from the DLP, and it circularly shifts the initial value 0/1/1/1. The third part is an operational amplifier (OP-amp) part. Because the A.C.

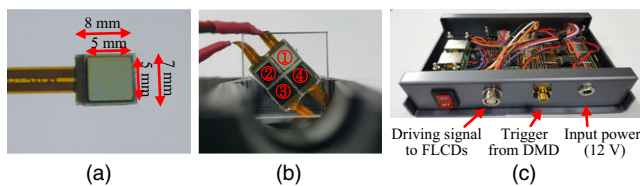


Fig. 6. (a) Dimensions of LC shutter, (b) 2×2 array of LC shutters, and (c) electronic box for synchronized control.

signal generated by the oscillator does not have enough power to turn off the LC shutter, it is amplified by the OP-amp circuits in front of the LC shutter.

IV. Computation of Hologram Suitable for Exit-Pupil Expansion

The CGH used for the exit-pupil expansion requires an angular spectrum with a bandwidth that is larger than that of the Nyquist region of the DMD. Figure 7 shows the positions of four filter apertures in the Fourier domain at 624 nm, 515 nm, and 425 nm respectively. Although the positions of the apertures are physically fixed independent of the wavelength, their positions are different from each other according to the wavelength when they are represented relative to high-order diffraction terms. For example, for the 624-nm wavelength, the first aperture is located in the second quadrant of the (3,4)-th order of diffraction, as shown in Fig. 7(a). However, for the 515-nm wavelength, the first aperture is located in the first quadrant of the (4,5)-th order of diffraction, as shown in Fig. 7(b). The relative positions of the filter apertures are summarized in Table 3.

Each CGH has information about the angular spectrum in the Fourier domain. When the part of the angular spectrum is chosen, it represents a view that is reconstructed at the viewpoint corresponding to the selected angular spectrum. In the exit-pupil expansion technique, the specific angular spectrum is larger than that of the Nyquist region of the DMD. The wave diffracted from the DMD has a repetitive angular spectrum with the period, which is two times that of the Nyquist frequency f_N . The exit-pupil expansion implies that an angular spectrum larger than the Nyquist region is represented by the given DMD with the help of sequential opening of filtering apertures. Therefore, by expanding the exit-pupil, the field of view of the system becomes wider than that of the conventional method. In this paper, the field of view is defined within the pupil of the human eye. Therefore, the expansion of the exit-pupil of

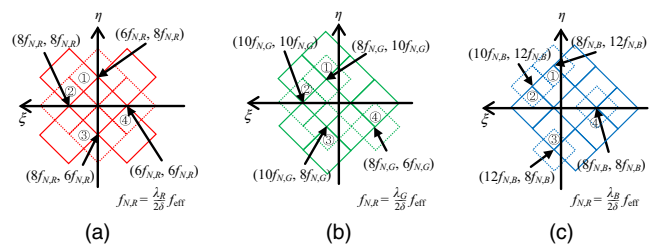


Fig. 7. Positions of four apertures relative to high-order diffraction terms in Fourier domain (a) at 624 nm, (b) at 515 nm, and (c) at 425 nm.

Table 3. Positions of single-sideband filters relative to diffraction orders.

Aper-ture	Red (624 nm)		Green (515 nm)		Blue (425 nm)	
	Diffraction order	Quadrant	Diffraction order	Quadrant	Diffraction order	Quadrant
1st	3rd, 4th	2nd	4th, 5th	1st	4th, 6th	3rd
2nd	4th, 4th	1st	5th, 5th	1st	5th, 6th	3rd
3rd	4th, 3rd	2nd	5th, 4th	3rd	6th, 4th	1st
4th	3rd, 3rd	4th	4th, 3rd	1st	4th, 4th	3rd

the system results in the enhancement of the accommodation effect felt by the observer.

The angular spectrum from the DMD is duplicated in the Fourier domain, and the angular spectrum selected by one aperture belongs to one quadrant of a high-order diffraction term. First, a hologram that is four times larger than the Nyquist region is computed. Next, the order of diffraction to which a portion of the angular spectrum corresponding to the aperture belongs is identified. Then, the specified order of diffraction is shifted to the origin of the angular spectrum. With the exception of the one where the portion corresponding to the aperture is positioned, the other three quadrants are removed. Finally, the only angular spectrum within the Nyquist region is inverse Fourier transformed to generate the CGH assigned to the filtering aperture.

Figure 8 shows the numerical reconstruction of the CGH based on exit-pupil expansion. The objects consist of five rings, as shown in Fig. 8(a). The smallest ring is placed at a distance of 1,100 mm from the eyepiece, and the second smallest ring is placed 1,000 mm from it. Because the virtual image of the hologram is designed to be positioned at 1,000 mm, these two small rings are near to the virtual image plane. Three large rings are made of relatively thin lines, and they are closely placed 100 mm from the eyepiece. As previously mentioned, there are four filter apertures in the Fourier domain. In Fig. 8(b), the area of the angular spectrum is four times larger than that of the Nyquist region. Here, black dots represent the order of the diffraction resulting from the pixel pitch of the DMD, and the blue dashed line refers to the Nyquist region. There are 950×950 sampling points, and the whole area in Fig. 8(b) requires $3,800 \times 3,800$ points. Therefore, the hologram is computed in the oversampling condition. Four apertures are distributed over the square drawn with a red dashed line. This area represents the expanded exit-pupil, and it is much larger than the maximum single-sideband filter, which is a half of the Nyquist region.

Figures 8(c)–(d) shows numerical reconstructions obtained by the CGH, which are images that propagate

to the virtual image plane. Therefore, the two smallest rings appear clearly, even though the surfaces of these objects are modeled in a random phase. Three rings

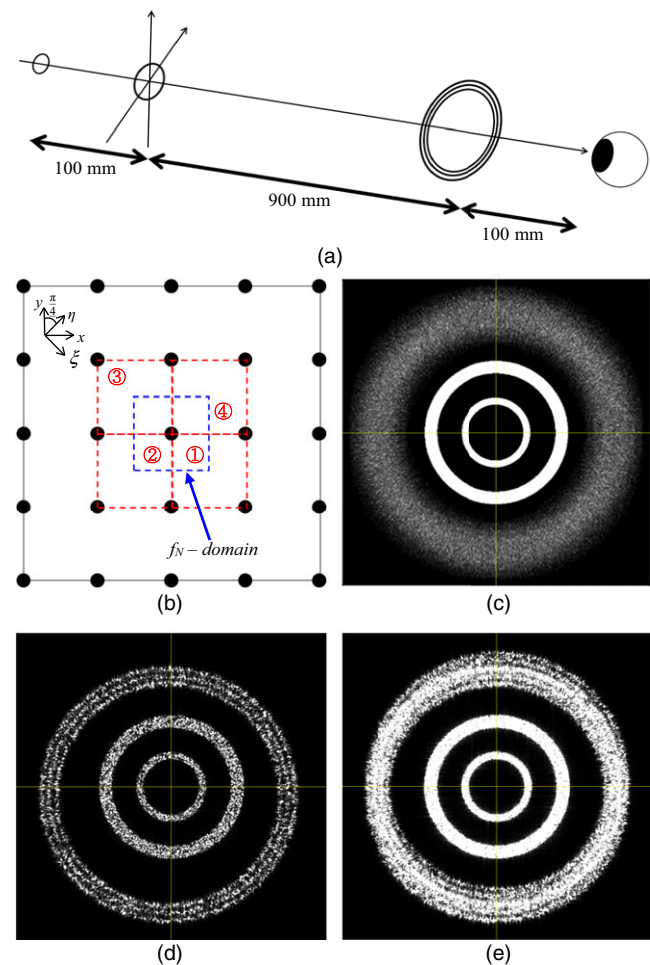


Fig. 8. Numerical reconstruction of CGH based on exit-pupil expansion. (a) Objects with five rings and (b) positions of filter apertures in Fourier domain. (c) Reconstruction image obtained using a CGH oversampled by four times with $3,800 \times 3,800$ points. (d) Reconstruction image obtained by the partial CGH with 950×950 points through the 4th aperture. (e) Sum of the intensities of four waves reconstructed by the CGHs through each aperture.

positioned at 100 mm appear seriously blurred, as shown in Fig. 8(c), owing to the large angular spectrum. It is expected that the accommodation effect depends on the bandwidth of the angular spectrum. The accommodation effect is not usually expected when the bandwidth is too small compared with the diameter of the pupil of the human eye. In our proposed system, the distance between adjacent orders of diffraction in the VW plane is 1.3 mm for a wavelength of 624 nm. Therefore, the size of the Nyquist region is not sufficient for an observer to feel the accommodation effect. When only the 4th aperture is open, the reconstruction image by one partial CGH is as depicted in Fig. 8(d). Here, three large rings are much clearer than those in Fig. 8(c). As discussed, the accommodation effect becomes weak according to the reduction of the bandwidth. In addition, these rings are decentered to the opposite direction of the position of the 4th aperture because this image was obtained through the aperture. Figure 8(e) shows the sum of the intensities of four waves that are sequentially reconstructed by the CGHs through each aperture. This image confirms that it is feasible for the exit-pupil expansion technique to provide an accommodation effect to observers more effectively. Because the waves are reconstructed sequentially, there is no interference between two waves from different apertures. Therefore, it appears to be similar to the result of the super multi-view display. In our proposed system, the VW of the holographic display is multiplexed within the pupil of the human eye, so our proposed system can be understood as a combination of a holographic display and a super multi-view display.

V. Experimental Result

Based on the optical layout design in Section II, we realized the expanded exit-pupil holographic HMD, as shown in Fig. 9. To reduce its form factor, two folding mirrors are inserted in front of the LC shutter array and the eyepiece. The DMD evaluation module with DLP3000 is modified and the projection optics is removed. The LED light sources are separated and the light is coupled into an optical fiber with a core size of 100 μm in order to control the spatial coherence. The dimension of the optics in this system is 180 mm \times 95 mm, and its height is 30 mm. The resultant size of the total system is 180 mm \times 170 mm \times 50 mm.

Because a single DMD is used in the color-sequential method, the full-color contents are provided by three CGHs with red, green, and blue wavelengths. In this paper, four apertures are selected, and LC shutters that are attached to them are opened one-by-one. Therefore, 12 CGHs are

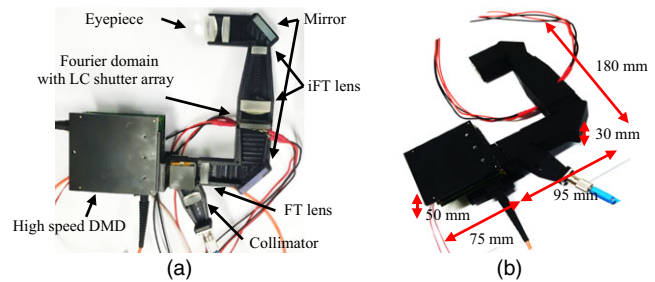


Fig. 9. (a) Structure and (b) dimensions of expanded exit-pupil holographic HMD.

required for our proposed system, and the set of RGB binary amplitude CGHs according to the positions of the apertures are depicted in Fig. 10. The object is designed as follows: the letter “K” is red, the letter “N” is green, and the letter “U” is blue. In addition, the depths of “K,” “N,” and “U” are 100 mm, 1,000 mm, and 1,100 mm, respectively. In addition, 12 CGHs are carefully computed corresponding to the proper single-sidebands of high-order diffraction terms depending on the wavelength. In this system, the off-the-shelf lenses listed in Table 1 are used, and the aberration needs to be carefully considered. Therefore, the CGHs have to be shifted depending on the position of the aperture considering the aberration of the lenses. The degree of the shifts is determined experimentally by measuring the incoherent imaging.

The reason for using edge-shape content in experiments is to show focusing and blurring clearly. There is no problem with the display of solid contents or general images in this proposed system. However, the quality of the contents is lower than that of a gray-scale hologram because it expresses content using a binary hologram. To overcome this problem, techniques that use several binary holograms with time-multiplexing have been studied to realize gray-scale [19], [20]. In this paper, we focus on the expansion of the exit-pupil of the holographic display instead of the improvement of the quality of individual holograms. Because the speed of the DMD is sufficiently high, it is possible to realize both techniques. That is, gray-scale holograms with time-multiplexing are represented, and they are assigned to four apertures.

The set of CGHs is uploaded to the driving board of the DMD in advance, and they are played sequentially. The exposure time of each CGH is set as 1.33 ms, and the total exposure time for 12 CGHs is 16 ms. The image is captured by a camera through the eyepiece. The exposure time of the camera is sufficiently larger than 16 ms, and the image is the summation of the intensities of every reconstructed wave. Figure 11 shows the captured images that are projected by the holographic HMD. The labels are

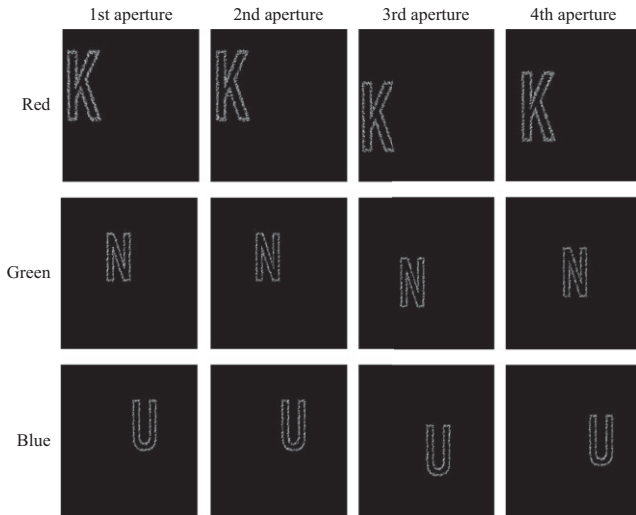


Fig. 10. Set of RGB binary amplitude CGHs according to the positions of the apertures.

positioned at 100 mm and 1,000 mm away from the eyepiece. Figures 11(a)–(c) show the results of reconstruction images when only the 1st aperture remains open. Here, the camera focuses at 100 mm, 1,000 mm, and 1,100 mm, respectively. In particular, “U” is projected with blue color, and it appears dark owing to the limited power of blue LEDs. Because “K” is the closest object from the eyepiece, it appears to be relatively large compared to “N” and “U.” Figures 11(d)–(f) show the results of reconstruction from 12 CGHs that are displayed synchronized with the opening of four apertures. In Fig. 11(d), the camera is set to focus at a distance of 100 mm, and the letter “K” is expected to be clear, while the letter “N” is expected to be blurred. However, in Fig. 11(e), the camera is set to focus at a distance of 1,000 mm, and the letter “N” is expected to be clear, while the letter “K” is expected to be blurred. However, the experimental results do not meet our expectation exactly because there are serious aberrations in our optics. In Fig. 11(d), the upper right part of the letter “K” is focused clearly, but the lower right part is not as clear owing to the noise. This noise mainly results from the CGHs passing through the 3rd aperture because some stray lights appeared when the 3rd aperture position was selected. Therefore, additional experiments were performed with only three apertures, with the exception of the 3rd aperture. The 3rd aperture is blocked and the images are taken, as shown in Figs. 11(g)–(i). As previously discussed in Fig. 11(d), the noise disappears at the lower right corner of the letter “K” in Fig. 11(g). In addition, “N” appears to be clear when the camera is focused at 1,000 mm. Even though

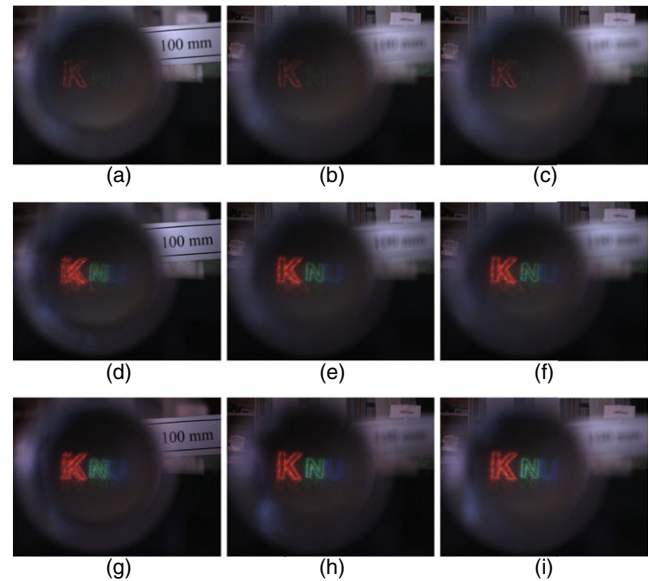


Fig. 11. Experimental results with the camera focused at different depths. When only the 1st shutter is opened, the images are captured with a focus at (a) 100 mm, (b) 1,000 mm, and (c) 1,100 mm. When four apertures are opened sequentially, the images are captured with a focus at (d) 100 mm, (e) 1,000 mm, and (f) 1,100 mm. When the three apertures, except for the 3rd aperture, are opened sequentially, the images are captured with a focus at (g) 100 mm, (h) 1,000 mm, and (i) 1,100 mm.

only three apertures are used to expand the exit-pupil, the size of the exit-pupil is much larger than the area of the Nyquist frequency. Therefore, we experimentally confirmed that it is feasible for the sequential opening of the single-sideband of high-order diffraction terms to increase the exit-pupil.

VI. Conclusion

Holographic HMDs usually have a narrow exit-pupil owing to the limitations of SBP, and it is difficult to provide a sufficient accommodation effect. In this study, we applied the time-multiplexing technique to improve the accommodation effect in a holographic HMD by expanding its exit-pupil. In the holographic HMD, the exit-pupil plane is the conjugate plane of the spatial filter plane. Therefore, the exit-pupil is expanded by opening several single-sidebands of the high-order diffraction terms sequentially. In this study, we implement the proposed system by synchronizing the high-speed DMD and LC shutter array. Experimentally, the feasibility is confirmed by expanding the exit-pupil to be four-times larger than the Nyquist frequency. For time-multiplexing, the DMD is used owing to its high-speed operation, but it has two main

disadvantages. One is that the oblique incident wave results in a shift of the undiffraction term, and it is difficult to choose regions that are suitable for spatial filtering among high-order diffraction terms. The other is that it generates a binary hologram, and the quality of the reconstructed wave is inevitably degraded. In the future, we plan to use a liquid crystal-on-silicon (LCoS) instead of the DMD in order to enlarge the size of the spatial filter and to improve the quality of the reconstructed wave.

Acknowledgments

This study was supported by the BK21 Plus project funded by the Ministry of Education, Rep. of Korea (21A20131600011), and was supported by “The Cross-Ministry Giga KOREA Project” grant funded by the Korea Government (MSIT) (No. GK17C0200, Development of full-3D mobile display terminal and its contents).

References

- [1] J. Hong et al., “Three-Dimensional Display Technologies of Recent Interest: Principles, Status, and Issues,” *Appl. Opt.*, vol. 50, no. 34, Nov. 2011, pp. H87–H115.
- [2] F.L. Kooi and A. Toet, “Visual Comfort of Binocular and 3D Displays,” *Displays*, vol. 25, no. 2, Aug. 2004, pp. 99–108.
- [3] D.M. Hoffman, A.R. Girshick, K. Akeley, and M.S. Banks, “Vergence-Accommodation Conflicts Hinder Visual Performance and Cause Visual Fatigue,” *J. Vision*, vol. 8, no. 3, Mar. 2008, pp. 1–30.
- [4] T. Shibata, J. Kim, D.M. Hoffman, and M.S. Banks, “Visual Discomfort With Stereo Displays: Effects of Viewing Distance and Direction of Vergence-Accommodation Conflict,” in *Proc. IS&T/SPIE Electr. Imag.*, San Diego, CA, USA, Aug. 12–16, 2012, pp. 78630P-1–78630P-9.
- [5] W.J. Tam, F. Speranza, S. Yano, K. Shimono, and H. Ono, “Stereoscopic 3D-TV: Visual Comfort,” *IEEE Trans. Broadcast.*, vol. 57, no. 2, Apr. 2011, pp. 335–346.
- [6] D. Drascic and P. Milgram, “Perceptual Issues in Augmented Reality,” in *Proc. SPIE*, Denver, CO, USA, Aug. 4–9, 1996, pp. 123–134.
- [7] Y. Takaki, “Super Multi-view Display and Holographic Display,” in *Proc. IEEE LEOS Annu. Meet. Conf.*, Belek-Antalya, Turkey, Oct. 4–8, 2009, pp. 12–13.
- [8] E. Moon, M. Kim, J. Roh, H. Kim, and J. Hahn, “Holographic Head-Mounted Display with RGB Light Emitting Diode Light Source,” *Opt. Express*, vol. 22, no. 6, Mar. 2014, pp. 6526–6534.
- [9] J.W. Goodman, *Introduction to Fourier Optics*, 3rd ed, Englewood, CO, USA: Roberts and Company Publishers, 2005.
- [10] A.W. Lohmann, R.G. Dorsch, D. Mendlovic, C. Ferreira, and Z. Zalevsky, “Space-Bandwidth Product of Optical Signals and Systems,” *J. Opt. Soc. Am. A*, vol. 13, no. 3, Mar. 1996, pp. 470–473.
- [11] H. Kim et al., “Anamorphic Optical Transformation of an Amplitude Spatial Light Modulator to a Complex Spatial Light Modulator with Square Pixels,” *Appl. Opt.*, vol. 53, no. 27, Sept. 2014, pp. G139–G146.
- [12] L. Onural, F. Yaras, and H. Kang, “Digital Holographic Three-Dimensional Video Display,” *Proc. IEEE*, vol. 99, no. 4, Apr. 2011, pp. 576–589.
- [13] M. Agour, C. Falldorf, and R.B. Bergmann, “Holographic Display System for Dynamic Synthesis of 3D Light Fields with Increased Space Bandwidth Product,” *Opt. Express*, vol. 24, no. 13, 2016, pp. 14393–14405.
- [14] J. Hahn, H. Kim, Y. Lim, G. Park, and B. Lee, “Wide Viewing Angle Dynamic Holographic Stereogram with a Curved Array of Spatial Light Modulators,” *Opt. Express*, vol. 16, no. 16, Aug. 2008, pp. 12372–12386.
- [15] F. Yars, H. Kang, and L. Onural, “Circular Holographic Video Display System,” *Opt. Express*, vol. 19, no. 10, 2011, pp. 9147–9156.
- [16] T. Kozacki, G. Finke, P. Garbat, W. Zaperty, and M. Kujawińska, “Wide Angle Holographic Display System with Spatiotemporal Multiplexing,” *Opt. Express*, vol. 20, no. 25, Dec. 2012, pp. 27473–27481.
- [17] Y. Takaki and Y. Hayashi, “Elimination of Conjugate Image for Holograms Using a Resolution Redistribution Optical System,” *Appl. Opt.*, vol. 47, no. 24, Aug. 2008, pp. 4302–4308.
- [18] Y. Lim et al., “360-Degree Tabletop Electronic Holographic Display,” *Opt. Express*, vol. 25, no. 22, Oct. 2016, pp. 24999–25009.
- [19] Y. Im, H. Kim, and J. Hahn, “Iterative Fourier Transform Algorithm Based on the Segmentation of Target Image for a High-Speed Binary Spatial Light Modulator,” *J. Opt. Soc. Kor.*, vol. 19, no. 2, 2015, pp. 149–153.
- [20] Y. Takaki and N. Okada, “Hologram Generation by Horizontal Scanning of a High-Speed Spatial Light Modulator,” *Appl. Opt.*, vol. 48, no. 17, 2009, pp. 3255–3260.



Mugeon Kim received his BS and MS degrees from the School of Electronics Engineering, Kyungpook National University, Daegu, Rep. of Korea, in 2014 and 2016, respectively, and he is currently pursuing his PhD degree from Kyungpook National University. His research focuses on head-mounted displays, head-up displays, and holographic displays.



Sungjin Lim received his BS and MS degrees from the School of Electronics Engineering, Kyungpook National University, Daegu, Rep. of Korea, in 2015 and 2017, respectively, and he is currently pursuing his PhD degree from Kyungpook National University. His research focuses

on 3D pick-up, 3D displays, and holographic displays.



Geunseop Choi received his BS degree from the School of Electronics Engineering, Kyungpook National University, Daegu, Rep. of Korea, in 2016, and he is currently pursuing his MS degree from Kyungpook National University. His research focuses on volumetric displays,

light-field displays, and holographic displays.



Youngmin Kim received his BS and Ph.D degrees in Electrical Engineering in 2005 and 2011, respectively, from Seoul National University, Rep. of Korea. After working at the same university as a postdoctoral researcher, he joined the Korea Electronics Technology Institute,

Seoul, Korea in 2011. His research focuses on interactive 3D displays, holographic displays, and visual fatigue associated with 3D displays.



Hwi Kim received the Ph.D. degree in 2008 from the School of Electrical Engineering, Seoul National University, Rep. of Korea. In 2010, he joined the Faculty of Electronics and Information Engineering, Korea University, Seoul, Rep. of Korea, where he is now an

associate professor. He has authored or co-authored more than 100 journal papers in the field of diffract optical field simulation for nano-structures and holographic devices.



Joonku Hahn received the Ph.D. degree in 2009 from the School of Electrical Engineering, Seoul National University, Rep. of Korea. In 2011, he joined the Faculty of Electronics Engineering, Kyungpook National University, Daegu, Rep. of Korea, and he is now an associate

professor. His main interests are 3D displays and digital holography applications.